



HAL
open science

Numerical modelling of the planetary adaptive optics mode of AOC, the adaptive optics project at Calern observatory

Benjamin Buralli, Olivier Lai, Marcel Carbillet, Lyu Abe, François-Xavier Schmider, Julien Dejonghe, Frantz Martinache, Éric Aristidi, Éric Cottalorda, Yves Bresson, et al.

► To cite this version:

Benjamin Buralli, Olivier Lai, Marcel Carbillet, Lyu Abe, François-Xavier Schmider, et al.. Numerical modelling of the planetary adaptive optics mode of AOC, the adaptive optics project at Calern observatory. SPIE Astronomical Telescopes + Instrumentation,, Jul 2022, Montréal, Canada. pp.337. hal-03790391

HAL Id: hal-03790391

<https://hal.science/hal-03790391>

Submitted on 28 Sep 2022

HAL is a multi-disciplinary open access archive for the deposit and dissemination of scientific research documents, whether they are published or not. The documents may come from teaching and research institutions in France or abroad, or from public or private research centers.

L'archive ouverte pluridisciplinaire **HAL**, est destinée au dépôt et à la diffusion de documents scientifiques de niveau recherche, publiés ou non, émanant des établissements d'enseignement et de recherche français ou étrangers, des laboratoires publics ou privés.

Numerical modelling of the planetary adaptive optics mode of AOC, the Adaptive Optics project at Calern observatory

B. Buralli, O. Lai, M. Carbillet, L. Abe, F.-X. Schmider, J. Dejonghe, F. Martinache, É. Aristidi, É. Cottalorda, Y. Bresson, J.-P. Rivet, D. Vernet, and F. Vakili

Laboratoire Lagrange, Observatoire de la Côte d’Azur/Université Côte d’Azur/CNRS, Bât. Fizeau, Parc Valrose, 06100 Nice, France

ABSTRACT

The AOC (Adaptive Optics at Calern) project is an adaptive optics bench being installed on one of the two 1-m telescopes of C2PU (Centre Pédagogique Planète Univers), situated in the Calern observatory, Observatoire de la Côte d’Azur, near Nice (France). AOC is installed at the Coudé focus of the telescope, and aims at working in the visible and near-infrared wavebands. The system is designed to work both in a standard stellar mode and in a more innovative planetary mode. Various visible and near-infrared outputs are provided, so that AOC can be used upstream of a number of scientific instruments. Early scientific applications are, on the one hand, development of post-AO short-exposure processing techniques (when used in the framework of the HiPIC project up to ~ 1600 nm), and, on the other hand, Jupiter oscillations (when used upstream of the JIVE/JOVIAL instrument at 519.6 nm). In addition to testing other concepts for imaging and interferometry, the facility will also be used for academic purposes, for instance in the framework of the Master program MAUCA. In this article we present the current status of the instrument, and in particular regarding the numerical modelling studies of its planetary wavefront sensing mode, with application to Mars and Jupiter.

Keywords: adaptive optics, wide-field sensing, planetary observation, numerical modelling

1. INTRODUCTION

AOC (Adaptive Optics at Calern) is the adaptive optics (AO) system installed and being developed at the C2PU (Centre Pédagogique Planète Univers), for one of its two 1-m telescopes, at the Calern plateau, near Nice (France). This system was designed to be able to work in both a stellar mode and a planetary mode. The stellar mode is meant to be a standard single conjugated AO (SCAO) mode, which measures the wavefront coming from a point source. In contrast, the planetary mode is a ground layer AO (GLAO) mode, conceived to work on extended sources, and more specifically planets of the solar system, such as Jupiter, Saturn and Mars. However, AOC has only one wavefront sensor (WFS), and will not make use of any laser guide star. From this aspect, the planetary mode is meant to be an innovative GLAO system taking the whole image of Jupiter, as large as $\sim 50''$, as the guide object in each lenslet of the 10×10 Shack-Hartmann matrix of the system.

AOC can then be used for different applications. For instance, the JOVIAL (Jupiter: Oscillations from Velocity Imaging At several Longitudes) project¹ will make use of the planetary mode of AOC as part of this ground-based network, in order to observe oscillations and atmospheric dynamics on Jupiter and potentially on other planets of the solar system. AOC is also an important necessity for the HiPIC (High angular resolution Post-adaptive optics Imaging at Calern observatory) project.² HiPIC is an imaging system which works in the visible and near-infrared domains in order to test high angular resolution imaging short-exposure techniques under different regimes of turbulence and subsequent AO correction. Eventually, the AOC system, as an addition to C2PU, will also be used as a new educational tool for the next generation of students in astrophysics, and possibly for demonstration to the public during open-door events.

2. SYSTEM DESCRIPTION

Figure 1 shows the layout of the AOC system implemented on an optical bench at the Coudé focus of the C2PU East telescope, Epsilon. The C2PU Epsilon telescope is an equatorial 1m telescope with two configurations, either a Cassegrain configuration or a f/31 Coudé focus, with two different M2 mirrors. The Coudé beam is sent in the mechanical axis by a removable M3 mirror and injected into the Coudé room by a M4 mirror. On the figure, the beam coming from the telescope is on the right side and it arrives on the table almost vertically. It is then reflected by a mirror M5 to reach the different sub-systems. At the focus of the Coudé beam, a controlled mirror ensure the stability of the pupil in the whole optical path, and in particular on the WFS.

In addition to the 10×10 Shack-Hartmann WFS, with 12×12 pixels under each sub-aperture, the system includes an ALPAO deformable mirror (DM), composed of 97 electro-magnetic actuators. A pupil image is formed on the DM through an off-axis parabola. The beam is then split into different wavelengths by a series of dichroic beam-splitters. The near-infrared part of the beam, above 900 nm, is selected before the WFS and sent to the Ninox camera, as part of the HiPIC instrument. Afterwards, another dichroic selects the light above 550 nm for wavefront sensing. The visible domain is then sent to the JIVE/JOVIAL instrument, and the blue part is sent to two cameras, one for the control of the pupil and the other showing the focal plane image.

The sensing field of view (FoV), due to a different pixel size of the detector, varies depending on the mode. In stellar mode, the pixel size is 0''6, resulting in a FoV of 7.2''. While in planetary mode, the pixel size is 5'', leading to a FoV of 60''. The detector used is an EMCCD Andor Ixon 860 camera (128×128 pixels, fast readout). The frequency of the system is 500 Hz, corresponding to a delay of 2 ms.

In addition, the table includes a calibration source which can be inserted in the beam through a motorized mirror. The source reproduce the pupil of the telescope, including the shadow of the M3 mirror and the spider. Two types of objects are available, one large source for the planetary WFS and a pin-hole source.

A derotator, not shown here, has been added to the system. It permits to compensate for the field rotation of the Coudé beam. In this way, the pupil remains fixed on the WFS, avoiding the need for a recalibration of the AO control when the spiders cross the sub-pupils.

The control software consists in a Python interface with a core realtime C++ code. The host computer is an Intel Xeon W-2275 3.3-GHz processor equipped with 14 physical cores (28 logical cores in Hyper-Threading mode), and a 16 GB-memory Windows 10 PC. The software uses a fast and versatile data exchange between the processes that is inherited from the SCExAO developments.

Figure 1 shows an optical scheme of the system (left) and a picture of it at the telescope (right).

3. SIMULATIONS

3.1 Simulation tools

This study was performed with two codes simultaneously: the latest version of the well-established CAOS tool, and an AOC-dedicated version of the GLAO simulation code `Instant_GLAO`.

CAOS (Code for Adaptive Optics Systems) is primarily a problem-solving environment, IDL-based and mainly composed of a global user interface and two Software Packages. One Software Package, the eponymous CAOS Software Package, is built in order to perform AO modeling. CAOS takes the form of a graphical interface in which one can select, place and parameterize the different modules corresponding to the different physical parts of the system. For example, the module ATM enables to set the parameters of the simulated atmosphere, such as the Fried parameter or the outer scale. SWS is the module corresponding to the Shack-Hartman WFS, with parameters such as the number of sub-apertures, the number of pixels per sub-aperture, or the pixel size. Each module is linked to a set of IDL scripts. By connecting all the necessary modules together, we get the full simulated system data flow, in an end-to-end manner.

`Instant_GLAO` is also based on IDL. But, contrary to CAOS, it is not freely distributed and is in constant evolution. While it was mainly been developed to simulate traditional (multiple guide stars) GLAO, it has been adapted to the AOC system in its GLAO planetary mode, but can also simulate its stellar mode. We hence used both codes to simulate the system in order to perform a comparative study, intervalidating the two codes

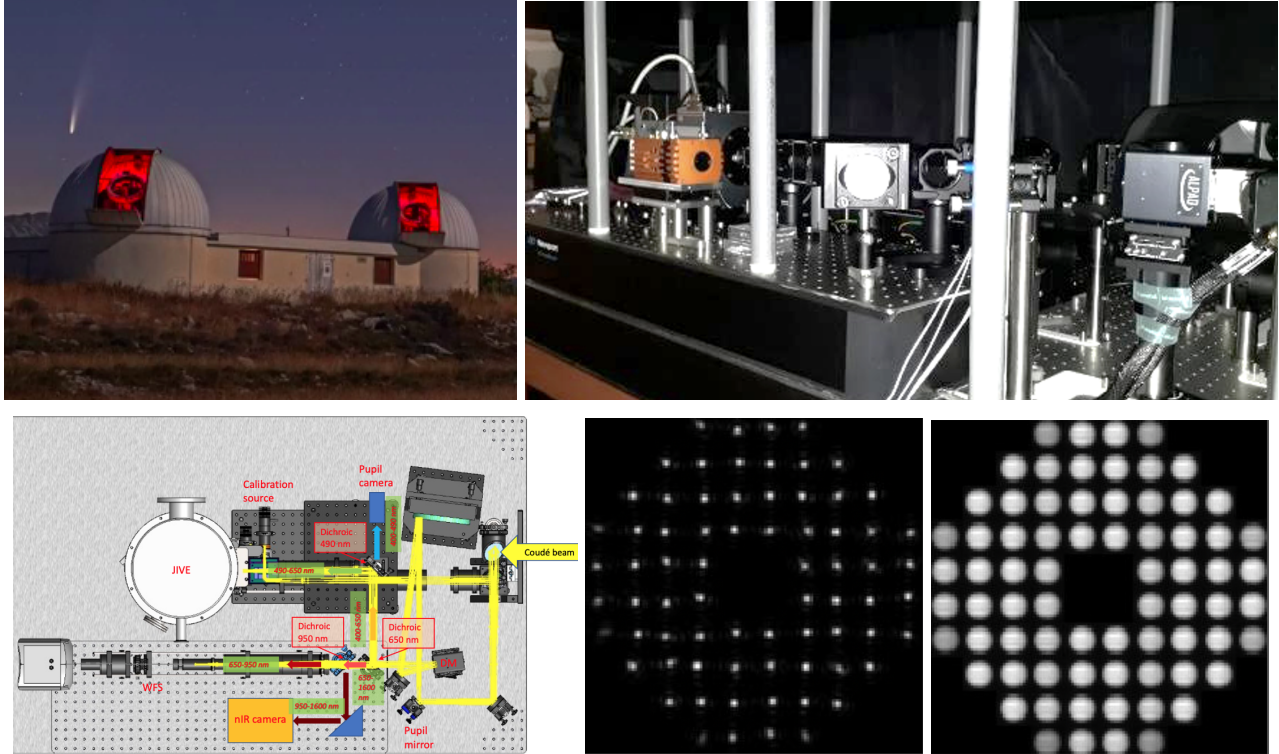


Figure 1. The AOC@C2PU bench. Top left: the C2PU telescopes. Top right: AOC at the Coudé focus of the C2PU Epsilon telescope. Bottom left: optical scheme of the system. Bottom right: the SH spots for, respectively, a point-like star (stellar mode) and Jupiter (planetary mode).

step by step, from a rather simple SCAO situation to a more complex planetary GLAO one involving a complex image such as a $50''$ wide picture of Jupiter.

3.2 Stellar mode

The stellar mode is designed to measure the turbulence along the line of sight to a guide star, i.e. a point source. It represents the classical SCAO mode of the system. In our case, it also works as a reference to compare the two codes and tune them, and to have a point of comparison for the planetary mode performance.

3.2.1 Ideal wavefront sensing

The first simulations were made with an ideal wavefront sensor within CAOS, the corresponding module IWS being an ideal component that will perfectly measure the wavefront perturbation (without noise) and correct from, here, the 14 first Zernike modes. It results in a single value corresponding to the minimal RMS we could theoretically reach. The reference RMS without correction is here of ~ 325 nm. When we apply the ideal AO WFS, its value drops to ~ 125 nm, which is compatible with the result when applying the Noll formula.³ This is hence our performance limit when considering 14 Zernike modes with this reference input.

3.2.2 Shack-Hartmann wavefront sensing

Technically speaking, the only difference between the stellar and the planetary modes is the plate scale. The number of pixels per sub-apertures remains the same, 12×12 . However, as we only need a small field in stellar mode, we use a fine sampling of $0''.6$ per pixel, resulting in a field of view of $7''.2$ for each sub-aperture.

For the atmospheric model, we set the Fried parameter r_0 to 6.9 cm and the outer scale L_0 to 100 m — neither of these numbers being optimistic ! In terms of the system itself, we looked at the optimisation of the loop gain and the exposure time of the Shack-Hartmann WFS. The loop gain, more specifically the integrator gain of the loop, is a parameter to set for the time constant of the integrator. The starting point for the simulations was

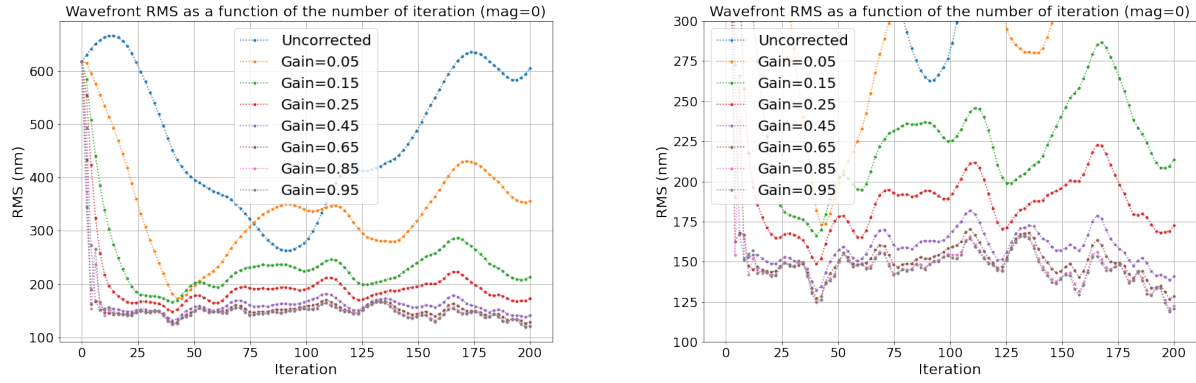


Figure 2. Phase screen RMS as a function of the integrator gain. The blue curve corresponds to the uncorrected case, for comparison. All the other curves corresponds to the RMS with correction, and with different gains from 0.05 to 0.95. All the data from the plots have been produced with a source magnitude of 0, which corresponds to a very high flux source. As it can be seen, when the gain increases, the RMS decreases and converges. On the right-hand plot, the low-value zone of the RMS has been zoomed in. It shows that the three curves corresponding to the gains 0.65, 0.85 and 0.95 are very similar and converge fast to low values of RMS. This range of gains is optimal in this configuration.

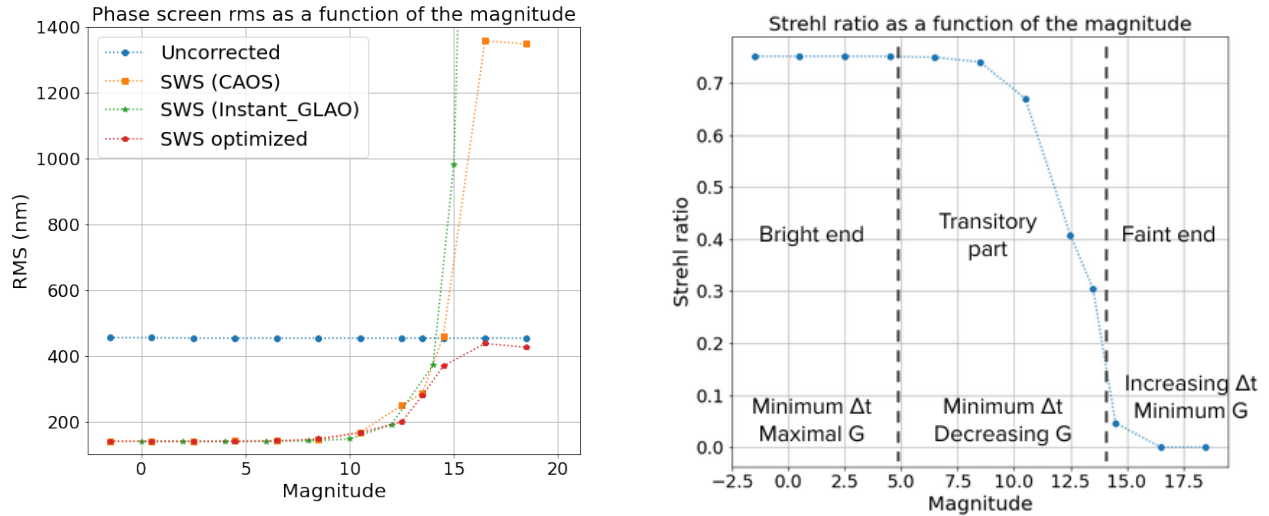


Figure 3. Left: phase screen RMS as a function of the source magnitude. The blue curve with filled circles corresponds to the mean uncorrected RMS. The orange curve with squares corresponds to the non-optimized corrected case, simulated with **CAOS**. The green curve with stars also corresponds to the non-optimized corrected case, but simulated with **Instant_GLAO**. The red curve with pentagrams corresponds to the case where the gain and the time exposure are optimized. Right: Strehl ratio as a function of the source magnitude. The Strehl ratio has been computed using the Maréchal approximation from the corrected phase screen RMS. The different regimes encountered are detailed.

a gain of 0.65, which seemed to work well for high flux sources on previous tests with **Instant_GLAO**. We then plotted the phase screen RMS as a function of time (i.e. loop iterations) for different gains in order to verify the optimal gain (see Fig. 2). Then we have to consider the exposure time for the spots of the WFS. By default, we considered the shortest exposure time possible, in our case 2 ms as the starting point for our simulations.

We then evaluated the level of correction as a function of the magnitude of the source. As for the previous subsection, we measured the residual phase screen RMS as the magnitude of the source increased, from 0 to 20. We plotted the data as a function of the magnitude, in both the corrected and uncorrected cases. The resulting graphs are displayed in the left plot of Fig. 3, which shows that the RMS for high flux sources (magnitude 0 to

10) is clearly better than in the uncorrected case, and it is even pretty close to the ideal WFS case.

However, starting from magnitude 10, the RMS begins to increase, and around magnitude 16, its value exceeds the RMS without correction. At this point, the system diverges and it degrades the residual RMS instead of improving it. However, in the case where we are using a Shack-Hartmann WFS, it may be possible to extend the performance a little bit by optimizing the exposure time, as well as the gain, for each point of the curve.

We optimised the gain for an exposure time of 2 ms, and when the loop diverged, we increased the exposure time as an attempt to stabilise it. We then had to re-optimize the gain for this new exposure time. The results are displayed in Fig. 3, where we considered the following magnitudes: 0, 2, 4, 6, 8, 10, 12, 14, 15, 16, 18, 20. The corresponding optimized gains and time exposure are respectively [0.95, 0.95, 0.95, 0.95, 0.95, 0.95, 0.65, 0.45, 0.45, 0.15, 0.05, 0.05], and [2, 2, 2, 2, 2, 2, 2, 2, 2, 2, 8, 8] ms.

One can observe that with the two parameters optimized, from around magnitude 12, the RMS is slightly lower than in the non-optimized case. But from magnitude 15, the difference is far more important. Actually, the system is no longer diverging, we are even below the uncorrected case.

From all this, we can notice that, for low magnitudes (high flux), the highest gains and the shortest exposure time are the optimal values (up to a gain of 0.95 at least). Then, as the magnitude increases (when the flux decreases), the optimal values are found by regularly decreasing the gain, but with the shortest exposure time. But when we reach the minimal gain, we can also optimize the values by increasing the exposure time. That is what is shown on the right plot of Fig. 3.

3.3 Planetary mode

3.3.1 Magnitude influence on the correction quality

The purpose of the planetary mode is to be able to perform GLAO on objects of the solar system, and more particularly planets as wide as Jupiter in opposition. The JIVE/JOVIAL project,¹ will make use of this system to perform measurements on Jupiter using this planetary mode. But the purpose is also to be able to use it for other extended objects of the solar system, such as Mars or Saturn. We are here basically simply using the fact that when guiding on an extended object, there is an intrinsic averaging of the high atmospheric layers resulting in a natural GLAO correction.

We report here on the testing the planetary mode with three different guiding objects: a uniform disk with the diameter of Mars (8"), another one with the diameter of Jupiter (~50"), and eventually a picture of Jupiter of the same angular size. We found that to compensate for the size of the object, more photons are needed to reach the same level of accuracy on centroid measurements and thus the same level of performance. This is clear from Fig. 4. As expected, we find that the limiting magnitude is lower than in the stellar case with the same gain of 0.65 and an exposure time of 2 ms (see the green and orange curves of Fig. 3), but, in the bright end, we reach the same level of performance.

For this figure, we started with a magnitude lower than 0, that is justified by the fact that Jupiter⁴ and Mars,⁵ when in opposition, have a magnitude between -1 and -2. For low magnitudes, up until around magnitude 3, the level of correction is the same as for the stellar mode. Then the RMS starts to grow up, but at different rates for each object. The correction is degrading faster for Jupiter than for Mars: at around magnitude 9 for Jupiter, and 11 for Mars, the corrected RMS is equal to the uncorrected one. Note by the way that we are here neglecting the anisoplanatism error. Let us focus on it on the next paragraph.

3.3.2 Anisoplanatism error

The anisoplanatism error is particularly important to consider when performing AO on wide fields. When we observe a point source, the wavefront is integrated along the line of sight in the atmosphere. However, when measuring a wavefront on extended objects, the light from different points does not travel exactly through the same volume of the atmosphere. Consequently, if we correct along only one specific line of sight on the object, an error on the correction will be induced on the rest of the object.

Usually when performing GLAO correction, multiple wavefront measurements are carried on different parts of the field. We use this method as a simplifying substitute to performing full 3D propagation on extended sources.

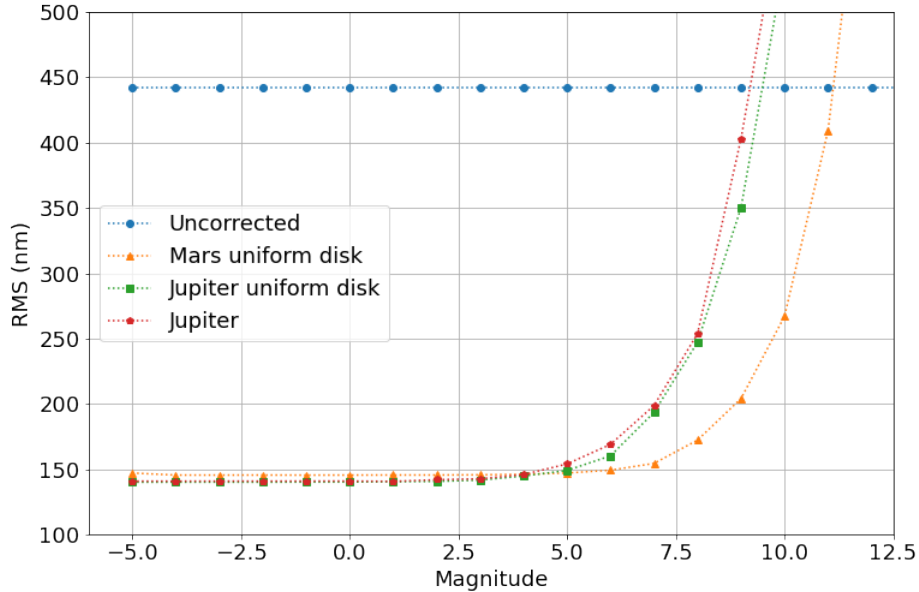


Figure 4. Phase screen RMS as a function of the source magnitude. The blue curve with round dots represents the uncorrected data. The orange curve with triangular dots corresponds to the RMS of the Mars uniform disk. The green curve with the square dots represents to the RMS of the Jupiter uniform disk. The red curve with pentagonal dots corresponds to the RMS of the Jupiter picture.

This opens up a free parameter, namely the number and positions of these virtual guide sources taken on the extended object. For example, for Mars, we took four points distributed on the surface of the disk. We then went a bit farther for Jupiter and tried three configurations: one with eight points, and two with nine points. Pictures of the points distribution on the images are shown in Fig. 5 and Fig. 6. These points correspond to the propagation points from which we perform wavefront sensing measurement.

A regular grid of 11×11 points is also used in order to estimate the correction quality across the scientific FoV, through a computation of the RMS along each of these 121 directions. We end up with an 11×11 array of RMS, from which we can build a 2D map of the correction over the FoV. We performed those simulations for the Mars uniform disk and the map of Jupiter. The results are displayed in Fig. 5 for Mars, and in Fig. 6 for Jupiter.

Different points on the disk representing the object all include the average of the atmospheric low layers which provides the GLAO correction. The effect of the high layers, which are different from one sub-aperture to another, is difficult to simulate accurately. So we made the simplifying assumption that the average of the centroids of the different points from the object is equal to the true mean centroid of each sub-image having undergone full 3D propagation. It is a way to simplify the GLAO correction simulation on an extended object by using point-like sources on the disk.

In the case of Mars (Fig. 5), the correction is better towards the center. If we compare the three RMS maps, we see that the system is converging pretty fast, even if the correction is slightly better and more homogeneous when we increase the number of iterations. However, as expected in GLAO, the correction at the center of the field is lower than in the case of single point correction due to the uncorrected high atmosphere.

In the case of Jupiter (Fig. 6), we considered three different configurations of source points. Contrary to the Mars case, we can see that with 200 iterations (0.4s of physical time), the system doesn't have the time to correctly converge. With 500 iterations (1s of physical time), the disk shape starts to show up, mostly for the second and third rows (nine source points). Then, for 1000 iterations (2s of physical time), the system seems

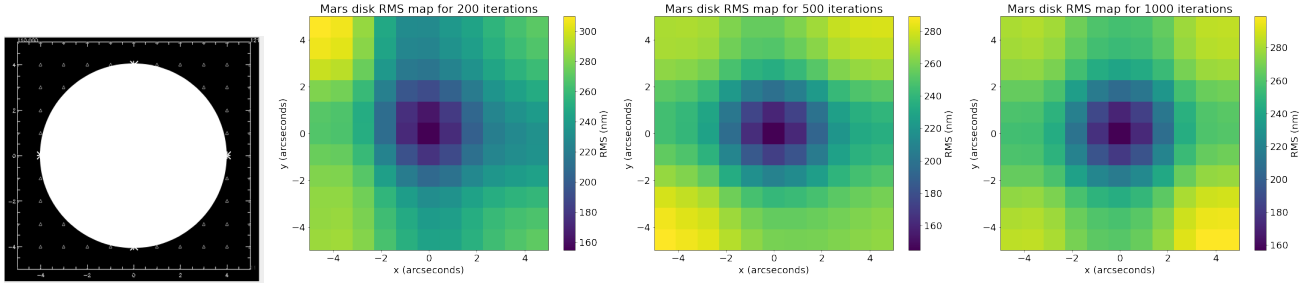


Figure 5. The most left picture represents the Mars uniform disk image we are using. The four crosses represent the points on which are performed the wavefront measurements. The 11×11 triangles correspond to the points on which is estimated the correction quality across the field. The three figures on the right are the resulting 2D RMS maps. Each pixel corresponds to one triangular measurement point on the left image. The x-axis and y-axis give the field dimension in arcseconds. The color maps of the 2D maps represent the RMS values in nm. The first 2D map has been made with a 200-iterations loop (400 ms), the second one with 500 iterations (1 s) and the third one with 1000 iterations (2 s).

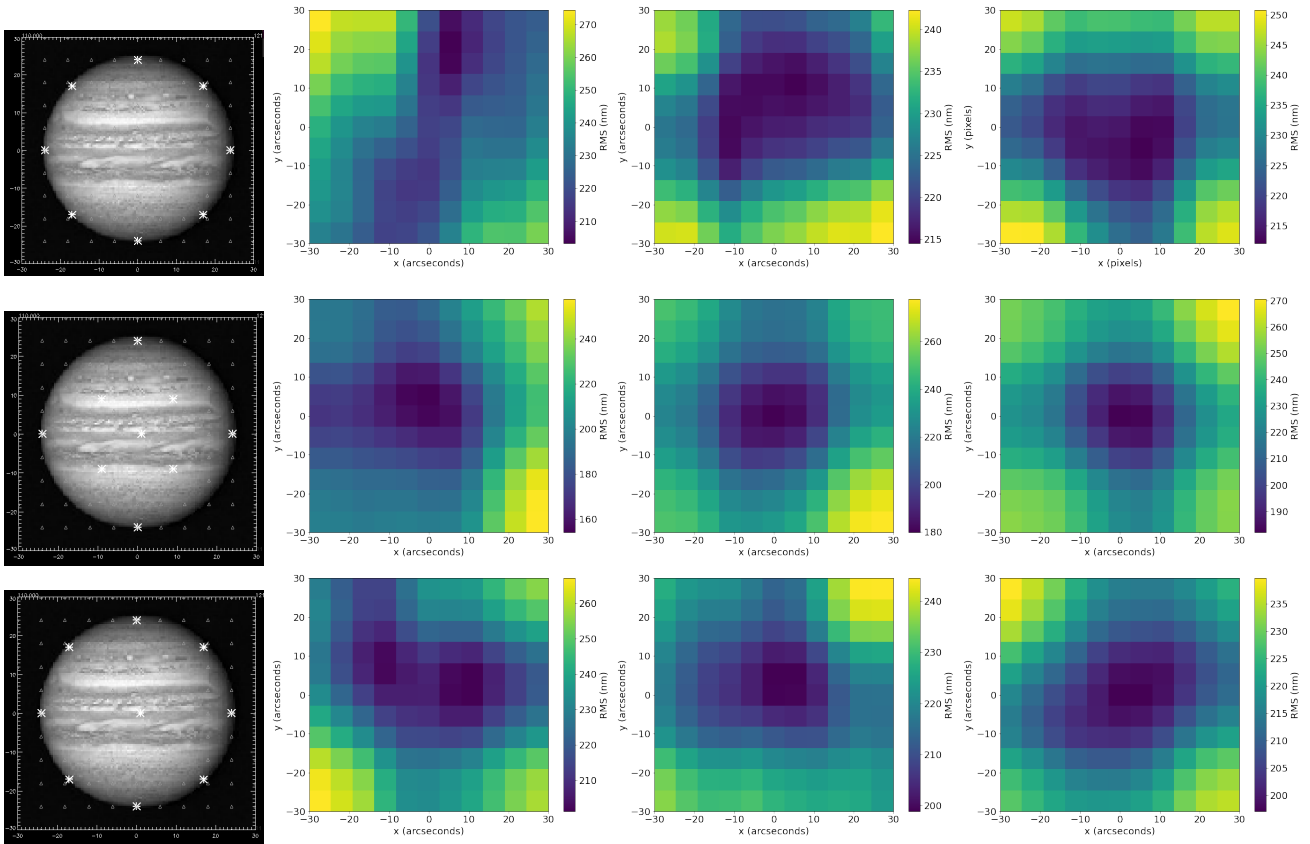


Figure 6. Same as Fig. 5, but each row corresponds here to a specific distribution of the crosses over the surface of the Jupiter map. First row: we here considered eight crosses distributed along the edge of the Jupiter map. Second row: we placed here nine crosses, four along the edges and five inside the disk, with one in the center. Third row: we also chose nine crosses here, but with eight distributed the same way as in the first row, and one in the center of the disk.

to have pretty much converge correctly in all three cases. But it seems that the correction is faster and slightly better when we are using nine points instead of eight for simulating the wavefront sensing. The overall correction is also less important than for the Mars case, which is not surprising considering that the object is wider, and its surface is definitely not uniform.

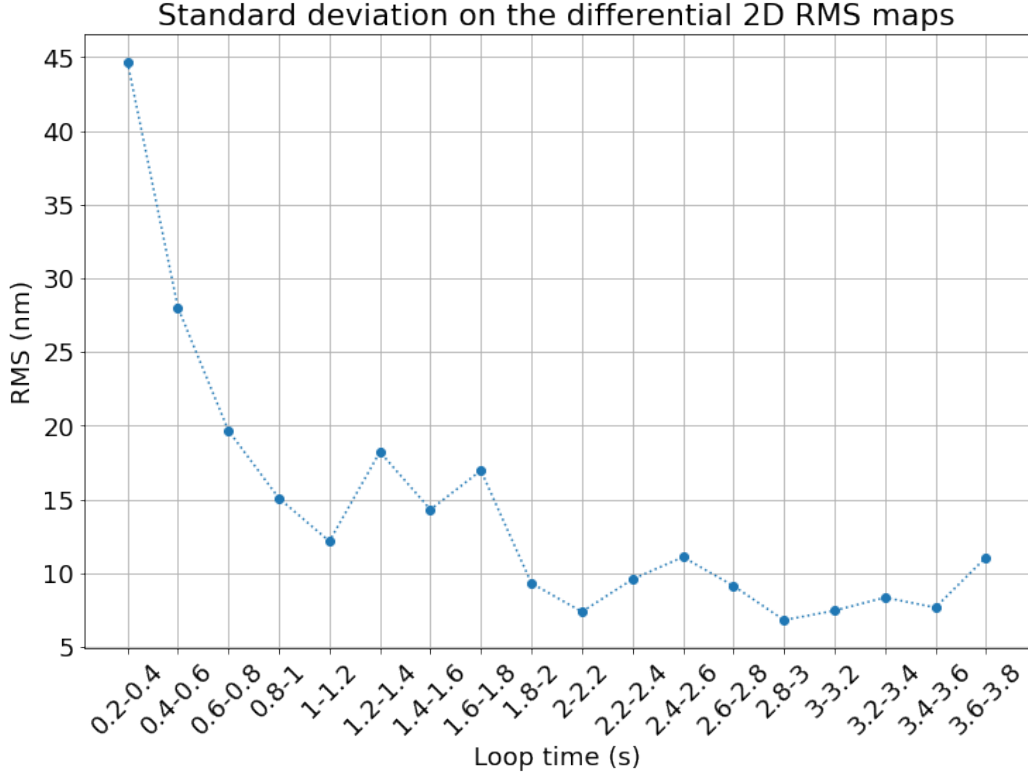


Figure 7. Phase screen RMS as a function of the loop time, Jupiter case. The simulation represents 3.8 s of time evolution, corresponding here to 1900 iterations.

3.3.3 Jupiter case: loop convergence time

We focus now on the Jupiter case, for which we noticed that it took a long time for the system to fully converge. We so selected the optimal configuration – the one shown in the second row of Fig. 6, and recovered the corrected RMS maps by range of 100 iterations (200 ms), up until 1900 iterations. Then we computed the differential 2D RMS maps by range of 100 iterations, the goal being to know how the RMS is evolving every 100 iterations. However, it is somehow tricky to analyse the convergence with 2D maps. Consequently, we chose to compute the standard deviation of each of the 2D maps. It results on a single value per range of 100 iterations. With those data, we plotted the evolution of the corrected RMS as a function of the loop time.

Figure 7 is so showing how the system is converging towards a corrected RMS threshold as the loop time is increasing. The curve is following the tendency we were expecting: the RMS is decreasing as the loop time is increasing, leading to convergence at some point. The fluctuations of the curve are due to the fact that the simulated atmospheric layers are evolving too as the time is increasing, hence the turbulence is not constant along the loop time. From the plot, we can estimate the loop time necessary to reach convergence to be as long as roughly 2 s (1000 iterations).

4. SUMMARY AND CONCLUSION

The purpose of this paper was to perform a simulation study of AOC, the AO system for one of the C2PU telescope at Calern observatory, near Nice (France). This system is installed at the telescope, but it still needs to be optimized to be fully operational, in particular in its planetary mode. AOC is an standard AO system, with a single DM and a 10×10 Shack-Hartmann WFS. It can work in two modes, a classical stellar mode, with a detector using 12×12 pixels of $0''.6$ in each sub-apertures, and a more innovative planetary mode, with pixels of $5''$. This last mode is designed to perform GLAO on extended objects such as Jupiter in opposition. Some projects are already planning to make use of this AO system, such as HiPIC² with its stellar mode, or JOVIAL¹

with its planetary mode. Being located in a facility also used for educational purposes, it will be an interesting addition for the student to work with, and for the public to see. Our study was mostly built on two goals: testing the performance of the system in its stellar mode and its planetary mode, but also to tune the two simulation codes that we used, CAOS and `Instant.GLAO`, in order to be able to perform a comparative study.

The different simulations we did in stellar mode showed that it performs as expected, providing a good correction for a large range of magnitudes. We also were able to enhance the performance by optimizing the gain and the exposure time of the system for each magnitude. The simulations confirmed that, as the magnitude increases (decreasing flux), optimal performance is achieved by first lowering the gain and keeping the lowest exposure time, and then, when one cannot decrease the gain anymore, by increasing the time exposure.

We then extended the simulations to the planetary mode on three extended objects, a uniform disk of 8'' diameter to simulate Mars, a uniform disk with a diameter of $\sim 50''$ to simulate Jupiter, and a picture of Jupiter. A preliminary study, without considering anisoplanatism, showed that we could achieve correction very close to the stellar mode one, but only at lower magnitudes. But it is not an issue when considering objects such as Jupiter which are rather luminous, at least at opposition. Then we introduced the anisoplanatism error to the simulations. The resulting 2D RMS maps we obtained showed how the correction evolves depending on the observed object, the distribution and number of source points on the surface of the disk, and the number of iterations. All those maps demonstrate that, in the frame of our study, the AO system is working well and providing good correction in planetary mode, in addition to the stellar mode.

From a simulation point of view, it is now necessary to progressively increase the complexity and realism of the simulations. We included the major steps effects, but now we can start focusing on realistic implementation issues. For example, the telescope central obstruction is not a perfect disk, it has an asymmetrical shape and the spider arms holding the secondary mirror rotate, changing the illuminated sub-aperture map during the observations.

In conclusion, let us say that the results shown on Jupiter are very promising for AOC in its planetary mode, but we need however to confirm that with on-sky observations.

REFERENCES

- [1] Gonçalves, I., Schmider, F.-X., Bresson, Y., Dejonghe, J., Preis, O., Robbe-Dubois, S., Appourchaux, T., Boumier, P., Leclec'h, J.-C., Morinaud, G., Gaulme, P., and Jackiewicz, J., "Advances in the development of a Mach-Zehnder interferometric Doppler imager for seismology of giant planets," in [*Ground-based and Airborne Instrumentation for Astronomy VI*], Evans, C. J., Simard, L., and Takami, H., eds., *Society of Photo-Optical Instrumentation Engineers (SPIE) Conference Series* **9908**, 99083M (Aug. 2016).
- [2] "HiPIC (High angular resolution Post-adaptive optics Imaging at Calern observatory)." <https://www.oca.eu/fr/lag-mpo-prog>.
- [3] Noll, R. J., "Zernike polynomials and atmospheric turbulence," *Journal of Optical Society of America* **66**, 207-211 (1976).
- [4] "Jupiter Fact Sheet." <https://nssdc.gsfc.nasa.gov/planetary/factsheet/jupiterfact.html>.
- [5] "Mars Fact Sheet." <https://nssdc.gsfc.nasa.gov/planetary/factsheet/marsfact.html>.